





- <sup>26</sup>Panjab University, Chandigarh, India  
<sup>27</sup>Delhi University, Delhi, India  
<sup>28</sup>Tata Institute of Fundamental Research, Mumbai, India  
<sup>29</sup>University College Dublin, Dublin, Ireland  
<sup>30</sup>Korea Detector Laboratory, Korea University, Seoul, Korea  
<sup>31</sup>SungKyunKwan University, Suwon, Korea  
<sup>32</sup>CINVESTAV, Mexico City, Mexico
- <sup>33</sup>FOM-Institute NIKHEF and University of Amsterdam/NIKHEF, Amsterdam, The Netherlands  
<sup>34</sup>Radboud University Nijmegen/NIKHEF, Nijmegen, The Netherlands  
<sup>35</sup>Joint Institute for Nuclear Research, Dubna, Russia  
<sup>36</sup>Institute for Theoretical and Experimental Physics, Moscow, Russia  
<sup>37</sup>Moscow State University, Moscow, Russia  
<sup>38</sup>Institute for High Energy Physics, Protvino, Russia  
<sup>39</sup>Petersburg Nuclear Physics Institute, St. Petersburg, Russia  
<sup>40</sup>Lund University, Lund, Sweden,  
 Royal Institute of Technology and Stockholm University, Stockholm, Sweden,  
 and Uppsala University, Uppsala, Sweden
- <sup>41</sup>Physik Institut der Universität Zürich, Zürich, Switzerland  
<sup>42</sup>Lancaster University, Lancaster, United Kingdom  
<sup>43</sup>Imperial College, London, United Kingdom  
<sup>44</sup>University of Manchester, Manchester, United Kingdom  
<sup>45</sup>University of Arizona, Tucson, Arizona 85721, USA
- <sup>46</sup>Lawrence Berkeley National Laboratory and University of California, Berkeley, California 94720, USA  
<sup>47</sup>California State University, Fresno, California 93740, USA  
<sup>48</sup>University of California, Riverside, California 92521, USA  
<sup>49</sup>Florida State University, Tallahassee, Florida 32306, USA
- <sup>50</sup>Fermi National Accelerator Laboratory, Batavia, Illinois 60510, USA  
<sup>51</sup>University of Illinois at Chicago, Chicago, Illinois 60607, USA  
<sup>52</sup>Northern Illinois University, DeKalb, Illinois 60115, USA  
<sup>53</sup>Northwestern University, Evanston, Illinois 60208, USA  
<sup>54</sup>Indiana University, Bloomington, Indiana 47405, USA  
<sup>55</sup>University of Notre Dame, Notre Dame, Indiana 46556, USA  
<sup>56</sup>Purdue University Calumet, Hammond, Indiana 46323, USA  
<sup>57</sup>Iowa State University, Ames, Iowa 50011, USA  
<sup>58</sup>University of Kansas, Lawrence, Kansas 66045, USA  
<sup>59</sup>Kansas State University, Manhattan, Kansas 66506, USA  
<sup>60</sup>Louisiana Tech University, Ruston, Louisiana 71272, USA  
<sup>61</sup>University of Maryland, College Park, Maryland 20742, USA  
<sup>62</sup>Boston University, Boston, Massachusetts 02215, USA  
<sup>63</sup>Northeastern University, Boston, Massachusetts 02115, USA  
<sup>64</sup>University of Michigan, Ann Arbor, Michigan 48109, USA  
<sup>65</sup>Michigan State University, East Lansing, Michigan 48824, USA  
<sup>66</sup>University of Mississippi, University, Mississippi 38677, USA  
<sup>67</sup>University of Nebraska, Lincoln, Nebraska 68588, USA  
<sup>68</sup>Princeton University, Princeton, New Jersey 08544, USA  
<sup>69</sup>State University of New York, Buffalo, New York 14260, USA  
<sup>70</sup>Columbia University, New York, New York 10027, USA  
<sup>71</sup>University of Rochester, Rochester, New York 14627, USA
- <sup>72</sup>State University of New York, Stony Brook, New York 11794, USA  
<sup>73</sup>Brookhaven National Laboratory, Upton, New York 11973, USA  
<sup>74</sup>Langston University, Langston, Oklahoma 73050, USA  
<sup>75</sup>University of Oklahoma, Norman, Oklahoma 73019, USA  
<sup>76</sup>Oklahoma State University, Stillwater, Oklahoma 74078, USA  
<sup>77</sup>Brown University, Providence, Rhode Island 02912, USA  
<sup>78</sup>University of Texas, Arlington, Texas 76019, USA  
<sup>79</sup>Southern Methodist University, Dallas, Texas 75275, USA  
<sup>80</sup>Rice University, Houston, Texas 77005, USA
- <sup>81</sup>University of Virginia, Charlottesville, Virginia 22901, USA  
<sup>82</sup>University of Washington, Seattle, Washington 98195, USA

(Received 8 January 2007; published 11 April 2007)

We have performed the first direct measurement of the time-integrated flavor untagged charge asymmetry in semileptonic  $B_s^0$  decays  $A_{\text{SL}}^{\text{s,unt}}$  by comparing the decay rate of  $B_s^0 \rightarrow \mu^+ D_s^- \nu X$ , where  $D_s^- \rightarrow \phi \pi^-$  and  $\phi \rightarrow K^+ K^-$ , with the charge-conjugate  $\bar{B}_s^0$  decay rate. This sample was selected from  $1.3 \text{ fb}^{-1}$  of data collected by the D0 experiment in run II of the Fermilab Tevatron collider. We obtain  $A_{\text{SL}}^{\text{s,unt}} = [1.23 \pm 0.97(\text{stat}) \pm 0.17(\text{syst})] \times 10^{-2}$ . Assuming that  $\Delta m_s/\bar{\Gamma}_s \gg 1$ , this result can be translated into a measurement of the  $CP$ -violating phase in  $B_s^0$  mixing:  $\Delta\Gamma_s/\Delta m_s \tan\phi_s = [2.45 \pm 1.93(\text{stat}) \pm 0.35(\text{syst})] \times 10^{-2}$ .

DOI: 10.1103/PhysRevLett.98.151801

PACS numbers: 13.20.He, 11.30.Er, 12.15.Hh, 14.40.Nd

This Letter presents the first measurement of a time-integrated flavor untagged charge asymmetry  $A_{\text{SL}}^{\text{s,unt}}$  in semileptonic  $B_s^0$  decays. This asymmetry is defined as

$$A_{\text{SL}}^{\text{s,unt}} = \frac{N(\mu^+ D_s^-) - N(\mu^- D_s^+)}{N(\mu^+ D_s^-) + N(\mu^- D_s^+)}, \quad (1)$$

where  $N(\mu^\pm D_s^\mp)$  is the number of decays  $B_s^0 \rightarrow \mu^\pm D_s^\mp \nu X$  integrated over the  $B_s^0$  lifetime. This asymmetry is called untagged because the initial flavor of the  $B_s^0$  meson is not determined.  $A_{\text{SL}}^{\text{s,unt}}$  is related to  $CP$  violation in  $B_s^0$  mixing [1] and can be expressed through the parameters of the  $B_s^0$  mass matrix as [2]

$$A_{\text{SL}}^{\text{s,unt}} = \frac{1}{2} \frac{x_s^2 + y_s^2}{1 + x_s^2} \frac{\Delta\Gamma_s}{\Delta m_s} \tan\phi_s, \quad (2)$$

where  $\Delta\Gamma_s$  ( $\Delta m_s$ ) is the width (mass) difference between the mass eigenstates in the  $B_s^0$  system,  $x_s = \Delta m_s/\bar{\Gamma}_s$ ,  $y_s = \Delta\Gamma_s/(2\bar{\Gamma}_s)$ , where  $\bar{\Gamma}_s$  is the average width in the  $B_s^0$  system, and  $\phi_s$  is a  $CP$ -violating phase. The standard model (SM) predicts a very small value for this asymmetry  $2 \times A_{\text{SL}}^{\text{s,unt}} = a_{\text{SL}}^s = (0.21 \pm 0.06) \times 10^{-4}$  [3], while the contribution of new physics can increase its magnitude up to the 1% level [4–6].

This measurement was performed using a large sample of semileptonic  $B_s^0$  decays collected by the D0 experiment at the Fermilab Tevatron collider in  $p\bar{p}$  collisions at  $\sqrt{s} = 1.96 \text{ TeV}$  and follows closely the procedure used in the estimate of the dimuon asymmetry described in Ref. [7]. The data correspond to an integrated luminosity of approximately  $1.3 \text{ fb}^{-1}$ . The D0 detector is described in detail elsewhere [8]. The detector components most important to this analysis are the central tracking and muon systems. The central tracking system consists of a silicon microstrip tracker (SMT) and a central fiber tracker (CFT), both located within a 2 T superconducting solenoidal magnet, with designs optimized for tracking and vertexing for pseudorapidities of  $|\eta| < 3$  and  $|\eta| < 2.5$ , respectively [9]. The outer muon system, with coverage for  $|\eta| < 2$ , consists of a layer of tracking detectors and scintillation trigger counters in front of 1.8 T iron toroids, followed by two similar layers after the toroids [10]. The polarities of the solenoid and toroids are reversed regularly during data taking, so that the four solenoid-toroid polarity combinations are exposed to approximately the same inte-

grated luminosity. The direct and reverse magnetic fields in the magnet were measured to be equal to within 0.1%. The reversal of magnet polarities is essential to reduce the detector-related systematics in asymmetry measurements and is fully exploited in this analysis.

The asymmetry  $A_{\text{SL}}^{\text{s,unt}}$  was measured using the decay  $B_s^0 \rightarrow \mu D_s \nu X$ , with  $D_s \rightarrow \phi \pi$ ,  $\phi \rightarrow K^+ K^-$ . The selection of this final state is described in detail in Ref. [11]. No explicit trigger requirement was made, although most of the sample was collected with single-muon triggers. Muons were required to have transverse momentum  $p_T(\mu) > 2 \text{ GeV}/c$  and momentum  $p(\mu) > 3 \text{ GeV}/c$ , to have hits in both the CFT and the SMT, and to have measurements in at least two layers of the muon system. All reconstructed charged particles in the event were clustered into jets [12], and the  $D_s$  candidate was reconstructed from three tracks found in the same jet as the reconstructed muon. Oppositely charged particles with  $p_T > 0.7 \text{ GeV}/c$  were assigned the kaon mass and were required to have an invariant mass  $1.004 < M(K^+ K^-) < 1.034 \text{ GeV}/c^2$ , consistent with that of a  $\phi$  meson. The third track was required to have  $p_T > 0.5 \text{ GeV}/c$ , a charge opposite to that of the muon charge, and was assigned the pion mass. The three tracks were required to have hits in the CFT and the SMT and to form a common  $D_s$  vertex using the algorithm described in detail in Ref. [13]. To reduce combinatorial background, the  $D_s$  vertex was required to have a positive displacement in the transverse plane, relative to the  $p\bar{p}$  collision point (or primary vertex), with at least  $4\sigma$  significance. The cosine of the angle between the  $D_s$  momentum and the direction from the primary vertex to the  $D_s$  vertex was required to be greater than 0.9. The trajectories of the muon and  $D_s$  candidates were required to originate from a common  $B_s^0$  vertex, and the  $(\mu D_s)$  system was required to have an invariant mass between 2.6 and  $5.4 \text{ GeV}/c^2$ .

To further improve the  $B_s^0$  signal selection, a likelihood ratio method [14] was utilized. Using background sidebands ( $B$ ) and sideband-subtracted signal ( $S$ ) distributions in the data, probability distributions were found for a number of discriminating variables. These variables were the angle between the  $D_s$  and  $K$  momenta in the  $K^+ K^-$  center-of-mass frame, the isolation of the  $(\mu D_s)$  system, the  $\chi^2$  of the  $D_s$  vertex, the invariant masses  $M(\mu D_s)$  and  $M(K^+ K^-)$ , and  $p_T(K^+ K^-)$ . The isolation was defined as the ratio of the sum of the momentum of the tracks used to reconstruct the signal divided by the total momentum of

the tracks contained within a cone with  $\sqrt{\Delta\eta^2 + \Delta\phi^2} < 0.5$  centered on the direction of the  $\mu D_s$  system. The final requirement on the combined selection likelihood ratio variable was chosen to maximize the predicted ratio  $S/\sqrt{S+B}$ .

For this analysis, we required the  $B_s^0$  vertex to have a positive displacement from the primary vertex to suppress the combinatoric background from the process  $c\bar{c}(b\bar{b}) \rightarrow \mu D_s \nu X$ , with the  $D_s$  originating from a  $b$  or  $c$  quark and the muon arising from another quark. The invariant mass distribution  $M(\phi\pi)$  for the selected events is shown in Fig. 1. The low and high peaks correspond, respectively, to  $(\mu D)$ , mostly due to  $B_s^0$ , and  $(\mu D_s)$ , mostly due to  $B_s^0$ . The curve represents a fit to the  $M(\phi\pi)$  spectrum. A single Gaussian was sufficient to describe the  $D \rightarrow \phi\pi$  decay and a double Gaussian to describe the  $D_s \rightarrow \phi\pi$  decay, and the background was modeled by an exponential. The total number of events passing all cuts in the  $D_s$  mass peak is  $27\,300 \pm 300$ (stat).

To measure  $A_{SL}^{v,unt}$ , both physics and detector effects contributing to the possible imbalance of events with positively and negatively charged muons must be taken into account. One physics source of asymmetry is  $CP$  violation in semileptonic  $B$  decays. In addition, forward-backward charge asymmetry of events produced in the proton-antiproton collisions can also be present. Detector effects can give rise to an artificial asymmetry if, e.g., the reconstruction efficiencies of positively and negatively charged particles are different. However, a positively charged particle produces the same track as a negatively charged particle in the detector with reversed magnet polarity. Therefore, almost all detector effects can be canceled, provided the fractions of events with opposite magnet polarities are approximately the same. This is the case in this analysis, where the exposures are the same within 1%.

According to the method described in Ref. [7], the event sample was divided into eight subsamples corresponding to all possible combinations of the toroid polarity  $\beta = \pm 1$ ,

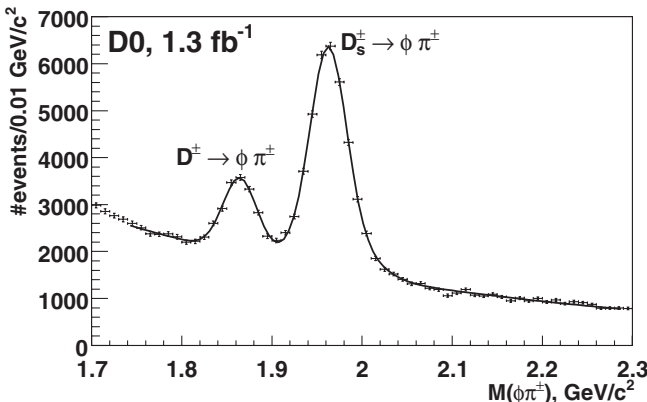


FIG. 1. The invariant mass distribution  $M(\phi\pi)$  for the selected  $B_s^0$  candidates. The curve shows the result of fit by a function described in the text.

the sign of the pseudorapidity of the  $(\mu\phi\pi)$  system  $\gamma = \pm 1$ , and the sign of the muon charge  $q = \pm 1$ . The number of  $(\mu D_s)$  events in each subsample was obtained by a fit to the mass distribution  $M(\phi\pi)$  using the same function as for the whole sample. For the cross-check, we also extracted the numbers of  $(\mu D)$  and background events from the fit. The widths and positions of the  $(\mu D_s)$  and  $(\mu D)$  peaks, the relative fractions of the two Gaussians describing the  $(\mu D_s)$  peak, as well as the background slope were fixed to the values obtained from the fit to the total  $M(\phi\pi)$  distribution. The numbers of  $(\mu D_s)$  and  $(\mu D)$  events,  $n_q^{\beta\gamma}(D_s)$  and  $n_q^{\beta\gamma}(D)$ , along with the number of the background events in the fitting range  $1.75\text{--}2.30\text{ GeV}/c^2$ ,  $n_q^{\beta\gamma}(\text{bkg})$ , for each subsample is given in Table I.

The fitted numbers of  $(\mu D_s)$  [ $(\mu D)$ , background] events were used to disentangle the physics asymmetries and the detector effects. The  $n_q^{\beta\gamma}$  can be expressed through the physics and the detector asymmetries as follows [7]:

$$n_q^{\beta\gamma} = \frac{1}{4}N\epsilon^\beta(1 + qA)(1 + q\gamma A_{fb})(1 + \gamma A_{det}) \\ \times (1 + q\beta\gamma A_{ro})(1 + q\beta A_{q\beta})(1 + \beta\gamma A_{\beta\gamma}). \quad (3)$$

Here  $N$  is the total number of  $(\mu D_s)$  [ $(\mu D)$ , background] events;  $\epsilon^\beta$  is the fraction of integrated luminosity with toroid polarity  $\beta$  ( $\epsilon^+ + \epsilon^- = 1$ );  $A$  is the integrated charge asymmetry to be measured;  $A_{fb}$  is the forward-backward asymmetry;  $A_{det}$  is the detector asymmetry for particles emitted in the forward and backward direction;  $A_{ro}$  is the range-out asymmetry that accounts for the change in acceptance of muons which bend towards the beam line and those which bend away from the beam line;  $A_{q\beta}$  is the detector asymmetry which accounts for the change in the muon reconstruction efficiency when the toroid polarity is reversed;  $A_{\beta\gamma}$  accounts for any detector-related forward-backward asymmetries that remain after the toroid polarity flip.

Since the system (3) contains eight equations, all six asymmetries together with  $N$  and  $\epsilon^+$  can be extracted for each of the three types of the events. Results are presented in Table II separately for  $(\mu D_s)$  and  $(\mu D)$  events and the

TABLE I. The numbers of events  $n_q^{\beta\gamma}(D_s)$  [ $n_q^{\beta\gamma}(D)$ ] in the  $D_s$  [ $D$ ] mass peak and in the background  $n_q^{\beta\gamma}(\text{bkg})$  for eight subsamples.

Subsample: $\beta\gamma q$	$n_q^{\beta\gamma}(D_s)$ (events)	$n_q^{\beta\gamma}(D)$ (events)	$n_q^{\beta\gamma}(\text{bkg})$ (events)
+++	$3216 \pm 76$	$907 \pm 55$	$9797 \pm 124$
+ - +	$3586 \pm 79$	$965 \pm 56$	$10\,387 \pm 127$
+ + -	$3391 \pm 78$	$1037 \pm 57$	$10\,390 \pm 127$
+ - -	$3225 \pm 76$	$963 \pm 55$	$9832 \pm 124$
- + +	$3616 \pm 80$	$1003 \pm 57$	$10\,508 \pm 128$
- - +	$3370 \pm 77$	$801 \pm 54$	$9987 \pm 125$
- + -	$3353 \pm 77$	$831 \pm 55$	$10\,215 \pm 125$
- - -	$3532 \pm 79$	$1116 \pm 59$	$10\,701 \pm 129$

TABLE II. The physics and detector asymmetries for  $(\mu D_s)$ ,  $(\mu D)$ , and background events. Uncertainties are statistical.

	$(\mu D_s)$	$(\mu D)$	Background
$N$	$27\,289 \pm 220$	$7623 \pm 162$	$81\,817 \pm 357$
$\epsilon^+$	$0.492 \pm 0.004$	$0.510 \pm 0.011$	$0.494 \pm 0.002$
$A$	$0.0102 \pm 0.0081$	$-0.0345 \pm 0.0211$	$-0.0056 \pm 0.0045$
$A_{fb}$	$-0.0046 \pm 0.0081$	$0.0480 \pm 0.0210$	$-0.0020 \pm 0.0043$
$A_{det}$	$-0.0051 \pm 0.0081$	$-0.0072 \pm 0.0212$	$0.0001 \pm 0.0044$
$A_{ro}$	$-0.0352 \pm 0.0081$	$-0.0819 \pm 0.0209$	$-0.0263 \pm 0.0044$
$A_{\beta\gamma}$	$-0.0097 \pm 0.0081$	$0.0104 \pm 0.0213$	$-0.0010 \pm 0.0044$
$A_{q\beta}$	$0.0030 \pm 0.0081$	$0.0014 \pm 0.0212$	$0.0046 \pm 0.0044$

background. The physics asymmetries  $A$  and  $A_{fb}$  for background events are consistent with zero. This is an important test for this method, since the precision of the asymmetry measurement for the background events is much higher than that of the signal due to the larger statistics. The largest detector asymmetry for all three types of the events is the range-out asymmetry.

It can be seen from (3) that if  $\epsilon^+ = \epsilon^- = 1/2$ , and the asymmetries  $A$ ,  $A_{fb}$ ,  $A_{det}$ ,  $A_{ro}$ ,  $A_{q\beta}$ , and  $A_{\beta\gamma}$  are small, each of them can be obtained independently by the appropriate division of the entire sample of events into two parts. For example, the asymmetry  $A$  can be obtained by dividing the sample according to the charge of muon. For such a division, and neglecting the second order terms, we obtain

$$A = \frac{n_+ - n_-}{n_+ + n_-}, \quad n_q = \sum_{\beta, \gamma=-1}^{+1} n_q^{\beta\gamma} \approx \frac{1}{2} N(1 + qA). \quad (4)$$

This observation explains, in particular, the similar values of statistical uncertainties for all asymmetries in Table II.

The resulting charge asymmetry of  $(\mu D_s)$  events is  $A = 0.0102 \pm 0.0081$  (stat). It is related to  $A_{SL}^{s,unt}$  via  $A = f_s A_{SL}^{s,unt} + f_d A_{SL}^{d,unt}$ , where  $f_s(f_d)$  is the fraction of  $B_s^0(B_d^0) \rightarrow \mu D_s \nu X$  decays in the  $(\mu D_s)$  sample.  $A_{SL}^{d,unt}$  may arise only from  $B_d^0 \rightarrow DD_s$  decay, the fraction of which in the  $(\mu D_s)$  sample was found to be small, at the level of  $(4 \pm 1)\%$ . Additionally, the value of  $A_{SL}^{d,unt}$  is strongly constrained experimentally [15,16] to be close to zero. Therefore, the time-integrated  $A_{SL}^{d,unt}$  component can be neglected. The fraction of  $B_s^0$  decays  $f_s$  was determined as follows. The decays  $B_s^0 \rightarrow \mu D_s \nu X$  and  $B_s^0 \rightarrow \tau D_s \nu X \rightarrow \mu D_s \nu X$  were considered as a signal. The decays  $B_s^0 \rightarrow D_s D_s \nu X$ , with  $D_s \rightarrow \mu \nu X$ , are not flavor-specific and, hence, were considered as a background. The decays  $B_d^0 \rightarrow DD_s \nu X$  were also included in the background. In addition, the process  $c\bar{c}(b\bar{b}) \rightarrow \mu D_s \nu X$  was taken into account. This background produces a pseudovertex, which peaks around the primary interaction point. It is reduced by approximately 50% by requiring a positive displacement of the  $(\mu D_s)$  vertex.

All processes were simulated using the EVTGEN [17] generator interfaced to PYTHIA [18] and followed by full modeling of the detector response using GEANT [19] and event reconstruction. The branching fractions of  $B_d^0$  decays were taken from Ref. [1], while the contribution of the process  $c\bar{c}(b\bar{b}) \rightarrow \mu D_s \nu X$  was measured directly in our data to be  $(5.9 \pm 1.7)\%$ . With these assumptions,  $(83.2 \pm 3.3)\%$  of the selected sample of  $(\mu D_s)$  events is composed of semileptonic  $B_s^0$  decays. The uncertainty on this value comes from the uncertainties on the branching ratios of the contributing  $B$  decays and the uncertainty on the fraction of the  $c\bar{c}(b\bar{b}) \rightarrow \mu D_s \nu X$  process in the sample. Taking into account the sample composition, the measured integrated charge asymmetry of semileptonic  $B_s^0$  decay is found to be  $A_{SL}^{s,unt} = [1.23 \pm 0.97(\text{stat})] \times 10^{-2}$ .

The following sources of systematic uncertainty were considered. The final state includes a  $K^+K^-$  pair. Therefore, the charge asymmetry of  $K$  meson reconstruction, which arises due to the different interaction cross sections of  $K^+$  and  $K^-$  in the detector material, does not contribute to the measured  $A_{SL}^{s,unt}$ . The charge asymmetry of pion reconstruction, however, can contribute. The  $\pi d$  interaction cross sections for positive and negative pions differ by  $(1.3 \pm 0.3)\%$  in the range 1–2 GeV/c [20]. Taking into account the amount of material which a pion crosses in the detector, the induced asymmetry due to pion reconstruction was estimated to be  $2 \times 10^{-4}$ . This value was included in the systematic uncertainty.

The uncertainty in the fraction of  $B_s^0$  signal in the  $(\mu D_s)$  sample produces a systematic uncertainty of  $1 \times 10^{-3}$ . This uncertainty also includes a possible residual variation of the signal fraction between subsamples.

The uncertainty due to the fitting procedure was estimated by varying the masses and widths of the peaks, and the slope of the background, by 1 standard deviation. The fitting procedure was also repeated with a single Gaussian describing the  $D_s$  peak and with a different fitting range. The resulting change of  $A_{SL}^{s,unt}$  did not exceed  $0.14 \times 10^{-2}$ , which was used as an estimate of the systematic uncertainty from this source.

The  $B_s^0$  reconstruction efficiency varies with the decay length due to the applied requirements. We verified that

this variation does not bias the result for  $A_{\text{SL}}^{\text{s,unt}}$  and the relation (2). In addition, any possible contribution of the  $B_d^0$  charge asymmetry to the measured value was estimated to be negligible.

Adding all contributions into the systematic uncertainty in quadratures, we obtain the resulting value of the time-integrated untagged charge asymmetry:

$$A_{\text{SL}}^{\text{s,unt}} = [1.23 \pm 0.97(\text{stat}) \pm 0.17(\text{syst})] \times 10^{-2}. \quad (5)$$

This is the first direct measurement of  $A_{\text{SL}}^{\text{s,unt}}$ . It can be seen that the statistical uncertainty dominates and will be improved in the future with the increase of statistics and addition of new decay modes. Using Eq. (2) and assuming that  $\Delta m_s/\bar{\Gamma}_s \gg 1$ , we obtain

$$\frac{\Delta\Gamma_s}{\Delta m_s} \tan\phi_s = [2.45 \pm 1.93(\text{stat}) \pm 0.35(\text{syst})] \times 10^{-2}. \quad (6)$$

This result is consistent with the SM prediction [3]. Its combination with the measurements of  $\Delta\Gamma_s$  [21],  $\Delta m_s$  [11,22], and dimuon charge asymmetry [7] provides a constraint on the  $CP$ -violating phase  $\phi_s$ . Such a combination, which is beyond the scope of this Letter, is described and presented in Ref. [23].

We thank the staffs at Fermilab and collaborating institutions and acknowledge support from the DOE and NSF (USA); CEA and CNRS/IN2P3 (France); FASI, Rosatom, and RFBR (Russia); CAPES, CNPq, FAPERJ, FAPESP, and FUNDUNESP (Brazil); DAE and DST (India); Colciencias (Colombia); CONACyT (Mexico); KRF and KOSEF (Korea); CONICET and UBACyT (Argentina); FOM (The Netherlands); PPARC (United Kingdom); MSMT (Czech Republic); CRC Program, CFI, NSERC, and WestGrid Project (Canada); BMBF and DFG (Germany); SFI (Ireland); The Swedish Research Council (Sweden); Research Corporation; Alexander von Humboldt Foundation; and the Marie Curie Program.

---

[1] W.-M. Yao *et al.* (Particle Data Group), J. Phys. G **33**, 1 (2006).

- [2] U. Nierste, hep-ph/0406300.
- [3] M. Beneke, G. Buchalla, A. Lenz, and U. Nierste, Phys. Lett. B **576**, 173 (2003); A. Lenz and U. Nierste, hep-ph/0612167.
- [4] Y. Grossman, Y. Nir, and R. Rattazzi, in *Heavy Flavours II*, edited by A. Buras and M. Lindner (World Scientific, Singapore, 1998).
- [5] F. Gabbiani, E. Gabrieli, A. Masiero, and L. Silvestrini, Nucl. Phys. **B477**, 321 (1996).
- [6] W. S. Hou, M. Nagashima, and A. Soddu, hep-ph/0610385.
- [7] V. Abazov *et al.* (D0 Collaboration), Phys. Rev. D **74**, 092001 (2006).
- [8] V. Abazov *et al.* (D0 Collaboration), Nucl. Instrum. Methods Phys. Res., Sect. A **565**, 463 (2006).
- [9] Pseudorapidity  $\eta$  is defined as  $\eta = -\ln[\tan(\theta/2)]$ , where  $\theta$  is the polar angle of the particle with respect to the proton beam direction.
- [10] V. Abazov *et al.*, Nucl. Instrum. Methods Phys. Res., Sect. A **552**, 372 (2005).
- [11] V. Abazov *et al.* (D0 Collaboration), Phys. Rev. Lett. **97**, 021802 (2006).
- [12] S. Catani *et al.*, Phys. Lett. B **269**, 432 (1991), “Durham” jets with the  $p_T$  cutoff parameter set at 15 GeV/c.
- [13] J. Abdallah *et al.* (DELPHI Collaboration), Eur. Phys. J. C **32**, 185 (2004).
- [14] G. Borisov, Nucl. Instrum. Methods Phys. Res., Sect. A **417**, 384 (1998).
- [15] B. Aubert *et al.* (BABAR Collaboration), Phys. Rev. Lett. **96**, 251802 (2006).
- [16] E. Nakano *et al.* (Belle Collaboration), Phys. Rev. D **73**, 112002 (2006).
- [17] D. J. Lange, Nucl. Instrum. Methods Phys. Res., Sect. A **462**, 152 (2001).
- [18] T. Sjöstrand *et al.*, Comput. Phys. Commun. **135**, 238 (2001).
- [19] CERN Program Library Long Writeup W5013 (1993); documentation available at <http://wwwasd.web.cern.ch/wwwasd/geant/>.
- [20] A. Carter *et al.*, Phys. Rev. **168**, 1457 (1968).
- [21] V. Abazov *et al.* (D0 Collaboration), Phys. Rev. Lett. **98**, 121801 (2007);  $\Delta\Gamma_s |\cos\phi_s|$  was measured in D. Acosta *et al.* (CDF Collaboration), Phys. Rev. Lett. **94**, 101803 (2005); V. Abazov *et al.* (D0 Collaboration), Phys. Rev. Lett. **95**, 171801 (2005).
- [22] A. Abulencia *et al.* (CDF Collaboration), Phys. Rev. Lett. **97**, 062003 (2006).
- [23] V. M. Abazov *et al.* (D0 Collaboration), hep-ex/0702030.